THE JOURNAL OF PHYSICAL CHEMISTRY Letters

Letter

Cite This: J. Phys. Chem. Lett. 2018, 9, 263−268

pubs.acs.org/JPCL

Photocurrent Spectroscopy of Perovskite Solar Cells Over a Wide Temperature Range from 15 to 350 K

Jay B. Patel, Qianqian Lin, Olga Zadvorna, Christopher L. Davies, Laura M. Herz, and Michael B. Johnston*

Department of Physics, University of Oxford, Clarendon Laboratory, Parks Road, Oxford OX1 3PU, U.K.

Supporting Information

ABSTRACT: Solar cells based on metal halide perovskite thin films show great promise for energy generation in a range of environments from terrestrial installations to space applications. Here we assess the device characteristics of the prototypical perovskite solar cells based on methylammonium lead triiodide ($CH_3NH_3PbI_3$) over a broad temperature range from 15 to 350 K (−258 to 77 °C). For these devices, we observe a peak in the short-circuit current density and open-circuit voltage at 200 K (−73 °C) with decent operation maintained up to 350 K. We identify the clear signature of crystalline PbI_2 contributing directly to the low-temperature photocurrent spectra, showing that PbI_2 plays an active role (beyond passivation) in $CH_3NH_3PbI_3$ solar cells. Finally we observe a blue-shift in the photocurrent spectrum with respect to the absorption spectrum at low temperature (15 K), allowing us to extract a lower limit on the exciton binding energy of 9.1 meV for $CH_3NH_3PbI_3$.

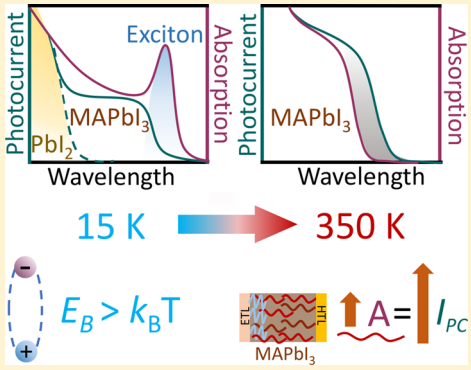

Photovoltaic devices containing a photoactive thin film of metal-halide perovskites have now achieved power conversion efficiencies above 22%,[1] while the prospect of multijunction perovskite cells promises even higher efficiencies.[2] High-performance solar cells are sought after for power generation in extreme environments such as space. However, to be suitable for use, e.g., on satellites, solar cells must be able to operate over a wide temperature range, typically from −100 to 125 °C (173 K − 398 K).[3] An in-depth understanding of perovskite solar cell operation over a wide range of temperatures is therefore crucial for the evaluation of their use in such locations. Methylammonium lead triiodide ($MAPbI_3$) is a prototypical metal-halide perovskite material whose use in solar cells has been extensively explored over the past five years. $MAPbI_3$ is well suited to photovoltaic applications owing to favorable intrinsic properties such as a high absorption coefficient for visible light, long charge-carrier diffusion lengths, high charge mobilities, and a benign defect chemistry.[4−6] Furthermore, the processing techniques available for thin-film fabrication of $MAPbI_3$ are truly versatile and offer the prospect of low-cost large-area photovoltaics. Spin-coating of a precursor solution containing PbI_2 and methylammonium iodide (MAI) has been the most popular of various solution processing techniques.[7−9] While spin-coating offers a low temperature method of processing, the thin films can suffer from the formation of pinholes and the choice of solvent can greatly affect film quality.[8] Thermal evaporation of the precursor materials, on the other hand, does not require extensive use of solvents and can reproducibly yield pinhole-free perovskite thin films, suitable for large area device fabrication.[10−12] In addition, the highest power conversion efficiency (PCE) for a $MAPbI_3$ based solar cell (20.3%) to date was achieved via a thermally evaporated $MAPbI_3$ active layer, which offers promise for facile manufacturing and commercialization of perovskite solar cells.[13] Both fabrication processes have shown that the perovskite thin films can be affected by any remnant precursors such as PbI_2 or MAI.[14,15] Recently, perovskite solar cells containing remnant PbI_2 in the perovskite thin film showed excellent PCE of 21.6%.[15] However, detailed analysis on the optoelectronic role of the remnant PbI_2 is not fully understood.

We have utilized the sensitive technique of Fourier transform photocurrent spectroscopy (FTPS) combined with current-density−voltage (J−V) measurements and absorption spectroscopy to assess the viability of $MAPbI_3$ solar cells over a temperature range from 15 to 350 K. The device characteristics, in particular, short-circuit current density and open-circuit voltage were optimal at 200 K, and devices operated well up to 350 K. However, a dramatic drop in photocurrent was observed for temperatures lower than 200 K, with photocurrents and photovoltages dropping rapidly toward very low temperatures (15 K). Interestingly, at low temperatures, we observe a characteristic contribution of PbI_2 in the $MAPbI_3$ device photocurrent spectra, which we identify by comparison with a PbI_2-only device with the same architecture. Moreover, we find that there is a discrepancy between the spectral onset of absorption and photocurrent (i) at low temperature, owing to the formation of excitons (ii) around

Received: November 4, 2017
Accepted: December 20, 2017
Published: December 20, 2017

DOI: 10.1021/acs.jpclett.7b02935
J. Phys. Chem. Lett. 2018, 9, 263−268

the orthorhombic-tetragonal phase transition as a result of mixed phases and (iii) at high temperature, because of enhanced collection of charge-carriers generated by longer wavelength light.

Figure 1 shows a cross-sectional scanning electron microscopy image of the device structure used for this study.

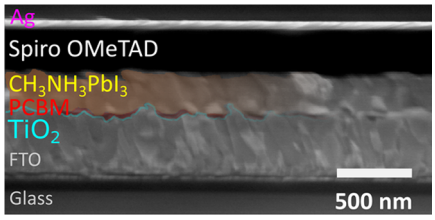

PCE (%)	J_{sc} (mAcm^{-2})	V_{oc} (V)	FF
10.92	17.86	1.07	0.57

Figure 1. SEM image showing the device structure used in this study, with the current−voltage characteristics measured under 1 sun illumination (AM 1.5G, 100 mW cm^{-2}).

The device was fabricated on a fluorinated-tin-oxide (FTO) coated glass substrate. It consisted of a dual TiO_2−PCBM electron extraction layer upon which the perovskite $MAPbI_3$ was deposited via coevaporation of MAI and PbI_2. A hole extraction layer of 2,2′,7,7′-tetrakis[*N*,*N*-di(4-methoxyphenyl)-amino]-9,9′-spirobifluorene] (Spiro OMeTAD) was spin-coated over the perovskite prior to thermal evaporation of a silver contact (full details of the device fabrication are provided in the Supporting Information). We have shown previously that this architecture produces high quality perovskite thin films and devices with minimal current−voltage hysteresis and high stabilized power output.[16] The devices were slowly cooled down to 4 K and then characterized as the temperature was increased incrementally. For all measurements, a tungsten halogen lamp was used as the light source.

To assess the device characteristics as a function of temperature, in situ short-circuit current density (J_{sc}) and open-circuit voltage (V_{oc}) of the $MAPbI_3$ device were measured between 15 and 350 K, with the results shown in parts a and b of Figure 2, respectively. The temperature dependence of the V_{oc} incorporates two different regimes, one above and one below 200 K, as observed previously when $MAPbI_3$ based devices had been cooled to 80 K.[20−24] The V_{oc} increases with temperature from 15 K and peaks at a value of 1.13 V at 200 K. The $J_{sc,}$ shows an even steeper increase of over 5 orders of magnitude with temperature, also peaking at 200 K. For temperatures higher than 200 K, the V_{oc} decreases again, similar to observations made for silicon and organic solar cells,[25−28] for which the effect has been attributed to the quasi-Fermi levels of the Boltzmann-like electron and hole populations moving closer together as the temperature is increased.[27,29,30]

To evaluate the effect of temperature-mediated changes in the structural disorder of the $MAPbI_3$ perovskite layer, we extracted the Urbach energy (E_u) from the photocurrent spectra.[31−33] Figure 2c shows the dependence of E_u (and hence disorder) as a function of temperature. To allow correlation with structural changes, we also indicate in shaded bars the temperature regions where $MAPbI_3$ is known to undertake structural phase transitions, i.e., from orthorhombic

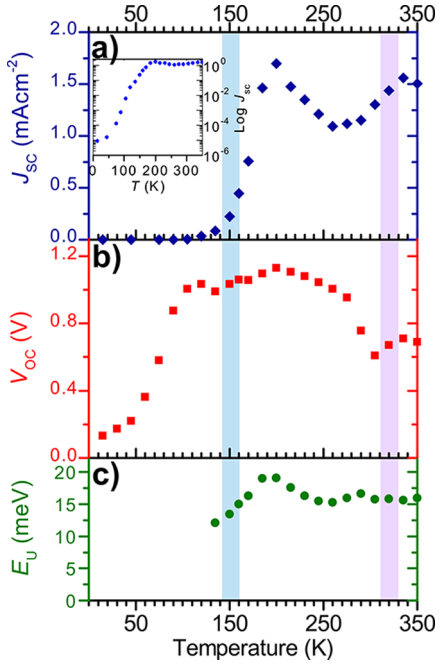

Figure 2. (a) Temperature dependence of the short-circuit current density for the $MAPbI_3$ device, with the inset showing the J_{sc} in a semilogarithmic scale. (b) Temperature dependence of the open-circuit voltage for the same device. (c) Temperature dependence of the Urbach energy (E_u) for the device derived from fits to external quantum efficiency spectra (as described in the Supporting Information (SI)). In situ temperature-dependent measurements were carried out using a tungsten halogen lamp with a light intensity of 0.29 sun. The shaded blue area shows the low-temperature phase transition from an orthorhombic to a tetragonal crystal structure.[17,18] The shaded lilac area shows the high-temperature phase transition from the tetragonal to the cubic perovskite crystal structure.[17,19] Temperature-dependent device characteristics of additional devices are presented in the SI.

to tetragonal at 140−160 K and from tetragonal to cubic near 310−330 K.[17−19] The value of E_u associated with the tetragonal phase of $MAPbI_3$ exhibited a minimum value of 12.1 meV at 135 K, and rose to a maximum value of E_u = 19.1 meV at 200 K before decreasing again to E_u = 16.7 meV at room temperature (290 K). In the cubic phase, the Urbach energy was found to be near 16 meV and insensitive to temperature. It was not possible to obtain E_u for the orthorhombic phase owing to the coexistence of small tetragonal domains.[18]

While thermal energy can play a direct role in dynamic structural disorder,[34,35] the nonmonotonic trend in E_u indicates that this is unlikely to be the major cause of the energetic broadening of the photocurrent onset here. Rather, it seems that additional changes with temperature, as for example strain, contribute to disorder. It is also interesting to note that the temperature dependence of the device J_{sc} and V_{oc} is not well correlated with the temperature dependence of the Urbach energy, indicating that disorder in the perovskite layer is unlikely to be the main factor limiting the low-temperature J_{sc} and V_{oc} of $MAPbI_3$ solar cells. We therefore suggest that the pronounced temperature variation in the J_{sc} and V_{oc} may in part be attributed to factors unrelated to the $MAPbI_3$ layer such as the charge-extraction performance of the electron- and hole-extractor layers. Hybrid perovskites such as $MAPbI_3$ have been found to exhibit enhanced charge-carrier mobilities with

DOI: 10.1021/acs.jpclett.7b02935
J. Phys. Chem. Lett. 2018, 9, 263−268

lower temperature[17] as a result of reduced electron−phonon coupling,[36] compatible with band transport within a large-polaron picture.[37] However, charge-transport in organic semiconductors and disordered crystalline solids, such as the TiO_2, PCBM, and Spiro OMeTAD materials typically used for charge-extraction for perovskite devices, is typically governed by hopping transport that may be thermally activated.[38,39] Jacobsson et al. observed a significant increase in series resistance from current−voltage scans, as the temperature decreased, confirming that the reduction in the conductivity of the organic charge transport layers leads to a decrease in J_{sc}.[22] Therefore, the sharp drop in J_{sc}, as the temperature is lowered past 150 K (Figure 2a) may potentially be partly remediated by use of alternative charge-extraction materials that exhibit band-transport at low temperatures, similar to $MAPbI_3$.

We are further able to use temperature-dependent measurements of photocurrent spectra to elucidate the role of excess PbI_2 in the performance of $MAPbI_3$ solar cells. A slight excess of PbI_2 in such devices has been shown previously to enhance the PCE.[15,40] It has been postulated that PbI_2 provides a crystalline framework which increases the crystal quality of $MAPbI_3$.[41] Furthermore, the presence of PbI_2 at grain boundaries has been found to be beneficial for device PCE.[42] However, the contribution of PbI_2 in to overall optoelectronic properties of the solar cell is still unclear. Room temperature measurements aimed to detect the photocurrent generated by PbI_2 have proven to be difficult as the high absorption coefficient of $MAPbI_3$ at 2.35 eV photon energy[14] (λ = 528 nm) masks any contribution from PbI_2.[43]

Figure 3a−c) shows snapshots of the photocurrent spectra of the $MAPbI_3$ device at 15, 150, and 290 K (blue solid lines). The spectra clearly show an energetic narrowing of the $MAPbI_3$ photocurrent onset from 290 to 15 K as a result of reduced electron−phonon coupling (thermal broadening).[36] In addition, the magnitude of the photocurrent, I_{PC}, increases substantially as the temperature is increased, in agreement with the already discussed behavior of the total current density, J_{sc}, observed in the current−voltage device characteristics (Figure 2). Interestingly, at low temperatures (15 K), an additional, sharp onset in photocurrent can be observed at 507 nm in the photocurrent spectra for the $MAPbI_3$ device (Figure 3a). This onset exhibits a red-shift with increasing temperature, reaching 510 nm at 150 K as shown in Figure 3b. The spectral position of the onset and the red-shift are comparable to those reported for the absorption onset of PbI_2.[35] Therefore, to verify that this contribution to the photocurrent indeed originates from PbI_2, we fabricated a photovoltaic device for which the $MAPbI_3$ layer was replaced by a PbI_2 layer. The photocurrent spectra of the PbI_2-only device at 15, 150, and 295 K are shown in Figure 3a−c as red dashed lines. The rise in photocurrent from the PbI_2 devices (red dashed lines) exactly matches the onset seen in the $MAPbI_3$ devices (solid blue lines) at 507 and 510 nm in Figure 3a,b, confirming the origin from PbI_2. We note that the presence of remnant crystalline PbI_2 in our $MAPbI_3$ layers is also supported by X-ray diffraction pattern (SI, Figure S10). At room temperature (Figure 3c), there is no obvious signature of a PbI_2 photocurrent onset in the $MAPbI_3$ device (blue line), most likely because the PbI_2 photocurrent is overwhelmed by the much stronger perovskite photocurrent at this temperature. Indeed, our photocurrent spectra for the PbI_2-only device (Figure 3, red dashed lines) clearly show that it can sustain a decent photocurrent between room temperature and 150 K,

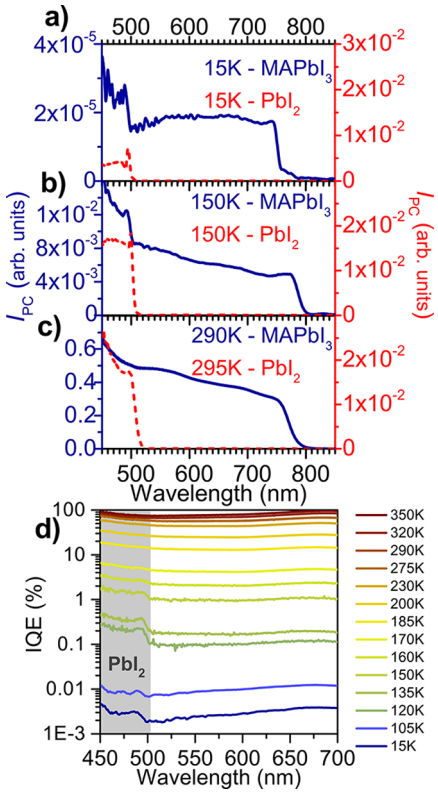

Figure 3. (a−c) Photocurrent spectra of a $MAPbI_3$ device as shown in Figure 1a (blue) and a PbI_2 device (red-dashed) which has the same architecture as the one shown in Figure 1a except that $MAPbI_3$ is replaced with PbI_2 at (a) 15 K, (b) 150 K, and (c) 290 K. The $MAPbI_3$ device at 15 and 150 K shows significant PbI_2 contribution to the photocurrent (I_{PC}) between 507 and 526 nm. Notably, the $MAPbI_3$ photocurrent increases by 4 orders of magnitude from 15 to 290 K, whereas the increase of PbI_2 photocurrent is smaller. (d) Internal quantum efficiency (IQE) spectra of the $MAPbI_3$ device from 15 to 350 K. At low temperatures, the PbI_2 contribution to the photocurrent is clearly visible. Notably, the IQE approaches 100% at high temperatures. Temperature-dependent photocurrent spectra of additional devices are presented in the SI .

but the photocurrent decreases as the temperature is reduced toward 15 K.

These results show that any remnant PbI_2 in the $MAPbI_3$ is able to play an active photocurrent generation role, even under normal operating conditions. Importantly, the $MAPbI_3$ device incorporates significantly less PbI_2 than $MAPbI_3$, yet it shows a clear signature in the photocurrent spectra at 510 nm. Additionally, between 160 and 120 K, the internal quantum efficiency (IQE) spectra for the $MAPbI_3$ perovskite solar cell (Figure 3d) are no longer flat, with higher IQE values at photon energies above 2.43 eV (λ < 510 nm). This demonstrates that the remnant PbI_2 becomes more efficient at converting absorbed light into photocurrent than $MAPbI_3$. However, below 120 K, the IQE spectra show a simultaneous decrease in IQE from both the PbI_2 and $MAPbI_3$. As mentioned earlier, this may be due to the loss in functionality of the organic charge transport layer due to an increase in series resistance at such low temperatures.[22]

Our observation of photogenerated current from PbI_2 networks within $MAPbI_3$ helps to explain previous reports that $MAPbI_3$ with a slight excess of PbI_2 improves solar cell performance.[15,40,41,44] Furthermore, Shih et al. have shown that

DOI: 10.1021/acs.jpclett.7b02935
J. Phys. Chem. Lett. 2018, 9, 263−268

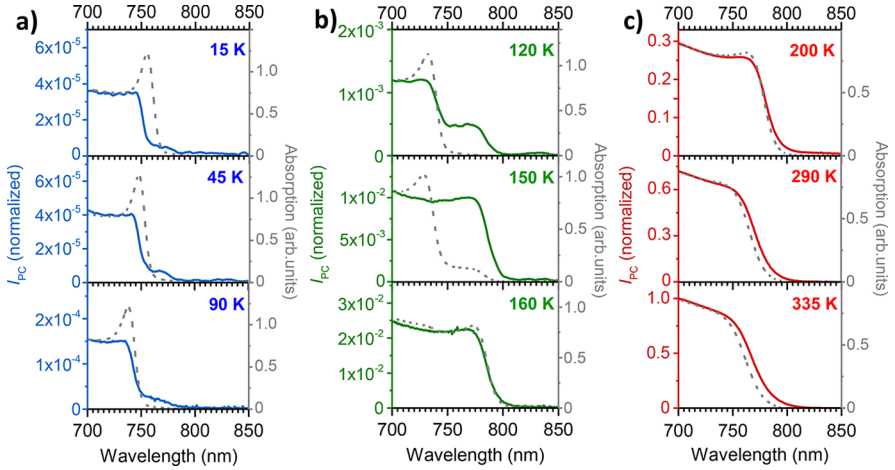

Figure 4. Temperature dependence of the photocurrent (I_{PC}) and absorption onset (dashed line) of the $MAPbI_3$ device. Here the reflection corrected absorption is of the full device architecture shown in Figure 1 without the Ag electrode. The photocurrent spectra were spectrally corrected using a calibrated silicon solar cell and normalized with respect to the 335 K spectrum. All measurements were made using a tungsten halogen light source. Full photocurrent spectra and absorption spectra can be found in Figures S1–S4 of the SI.

$MAPbI_3$ devices with excess PbI_2 perform better when the PbI_2 is on the surface of the $MAPbI_3$ perovskite grain.[45] On the basis of the collective data presented, there are two processes that could occur, either concurrently or separately, to explain the PbI_2 signal shown in Figure 3. First, there could be a homogeneous network of PbI_2 through which photogenerated charge-carriers can be transported and then collected at electron and hole selective layers, which is possible as shown by the PbI_2-only device. Second as Holovský et al. have postulated, PbI_2 may create a type II heterojunction with the $MAPbI_3$, making it energetically more favorable for the holes to be transported into the $MAPbI_3$ and electrons to be transported into the PbI_2.[45,46] However, this process is thermally activated,[46] hence at low temperatures it will not be as effective. Our results imply that at low temperature, remnant PbI_2 in a $MAPbI_3$ device can produce photocurrent independent of $MAPbI_3$ and at room temperature PbI_2 is also capable of generating photocurrent. To understand the exact origin of the photocurrent observed of PbI_2 at different temperatures, in $MAPbI_3$ thin film devices, would require detailed investigation of the interface between $MAPbI_3$ and PbI_2.

We may further deduce information on the operation of the $MAPbI_3$ photovoltaic device by contrasting the temperature-dependent photocurrent and absorption near their onsets (Figure 4). For this purpose, absorption spectra were taken of a film whose architecture resembles that of the device shown in Figure 1 but without the silver electrode. We are able to identify three different regimes of contrasting behavior. Over the temperature range of 160–120 K (Figure 4b), we observe a significant blue-shift in the absorption spectrum which is characteristic of the tetragonal to orthorhombic phase transition in $MAPbI_3$, as previously observed in isolated $MAPbI_3$ films.[17] However, the photocurrent onset over this range shows that $MAPbI_3$ retains remnant tetragonal phase in the device that evidently generates an effective photocurrent. Even though the absorption spectra only indicate a small quantity of remnant tetragonal $MAPbI_3$, a significant amount of red-shifted photocurrent onset can be observed near the energy associated with the band gap of the tetragonal phase. Such remnants of the tetragonal phase $MAPbI_3$ must therefore be able to form a crystalline network that allows for photogenerated charges to be extracted at low temperatures. Figure 4a shows that in the temperature range from 15 to 90 K, the photocurrent onsets become dominated by a trade-off between free-charge and exciton formation. In this temperature range, there is a significant blue-shift of the photocurrent onset compared to the absorption onset and the absorption onset shows notable excitonic absorption features. Therefore, in a device that is under no bias, i.e., under short circuit conditions, there would be negligible photocurrent contribution from dissociated excitons unless the thermal energy exceeds the exciton binding energy.[47] Thus, by comparing the peak of the exciton and the onset of photocurrent at low temperature, as shown in SI, Figure S9, we can estimate a lower bound on the exciton binding energy (E_B) at 15 K to be 9.1 meV, which is consistent with previous magneto-optical experiments which found a value of E_B = 16 meV at 4 K.[47] In contrast, for temperatures above 160 K, the photocurrent onset first overlaps with the absorption onset, then even shifts to slightly longer wavelength (Figure 4c). Hence in this temperature range, photoexcitation yields mostly free charges, as confirmed by our Saha–Langmuir analysis (presented in SI, Figure S7).[48,49] At temperatures above 160 K, excitons have sufficient thermal energy to dissociate, allowing photocurrent to be generated from dissociated electrons and holes. Curiously, we find that the onset of the photocurrent is slightly red-shifted in relation to the onset of the absorption for temperature above 290 K, which we attribute to an optical cavity effect within the perovskite multilayer device.[50−52] Because the absorption coefficient of $MAPbI_3$ is high for photons well above its bandgap, a high charge-carrier density is photogenerated mainly on the side of the perovskite layer closest to the semitransparent contact (FTO).[50,53] However, longer-wavelength photons near the band-edge will generate a much more uniform charge density profile through the $MAPbI_3$ layer, and it has been observed previously that uniform charge distributions can result in more effective collection of photocurrent in $MAPbI_3$ compared with when electron–hole generation is concentrated close to just one $MAPbI_3$ interface of a planar heterojunction device.[50,51,54] Thus, the photocurrent spectra exhibit an enhanced contribution toward the low-energy side of the perovskite bandgap. Therefore, the correlation between photocurrent and absorption spectra

DOI: 10.1021/acs.jpclett.7b02935
J. Phys. Chem. Lett. 2018, 9, 263−268

provides an illuminating insight into the mechanisms by which absorbed photons are converted to photocurrent.

In conclusion, the temperature-dependent J_{sc} and V_{oc} for a $MAPbI_3$ solar cell have been tracked from 15 to 350 K. We observe that both the J_{sc} and V_{oc} peak near 200 K, whereafter they deteriorate steeply at lower temperatures but only decrease gradually toward higher temperatures. We have probed the device with the highly sensitive technique of Fourier transform photocurrent spectroscopy to understand the temperature dependence of the photocurrent spectra. By comparing photocurrent spectroscopy and absorption spectroscopy on the same solar cell architecture, we estimate the exciton binding energy for $MAPbI_3$ to be greater than 9.1 meV at low temperature and show that, at higher temperatures, low-energy photons that generate uniform charge-density profiles dominate the photocurrent onset. Furthermore, photocurrent spectroscopy has proven a vital tool for understanding the influence of remnant precursors in the perovskite to the total device photocurrent. We show that PbI_2 may contribute to the total photocurrent of the device, hinting at the role of remnant PbI_2 in the $MAPbI_3$ thin films. Overall, $MAPbI_3$ solar cells have shown optimal device parameters at −73 °C, which shows that only small improvements may be required in the device architecture to render these solar cells a viable, cheaper alternative for space applications. With the advent of perovskite semiconductors consisting of many mixtures of cations, metals, and halides, further investigation will be helpful to see how compositional differences, as well as changes in charge extraction layer materials, may affect the temperature-dependent device performance.

■ ASSOCIATED CONTENT

Supporting Information

The Supporting Information is available free of charge on the ACS Publications website at DOI: 10.1021/acs.jpclett.7b02935.

Details on device fabrication, Fourier transform photocurrent spectroscopy, X-ray diffraction, scanning electron microscopy, Fourier transform infrared spectroscopy, further temperature dependent measurements, Urbach energy fits, device performance metrics, and the fraction of free charges vs excitons (PDF)

■ AUTHOR INFORMATION

Corresponding Author

*E-mail: michael.johnston@physics.ox.ac.uk. Website: www-thz.physics.ox.ac.uk.

ORCID

Laura M. Herz: 0000-0001-9621-334X

Michael B. Johnston: 0000-0002-0301-8033

Notes

The authors declare no competing financial interest.

■ ACKNOWLEDGMENTS

We gratefully acknowledge financial support from the Engineering and Physical Sciences Research Council (UK) (EPSRC). We thank Rebecca Milot and Adam Wright for helpful discussions. J.B.P. thanks the EPSRC and Merck Chemicals for financial support through an industrial CASE studentship.

■ REFERENCES

(1) Yang, W. S.; Park, B.-W.; Jung, E. H.; Jeon, N. J.; Kim, Y. C.; Lee, D. U.; Shin, S. S.; Seo, J.; Kim, E. K.; Noh, J. H.; et al. Iodide Management in Formamidinium-Lead-Halide–based Perovskite Layers for Efficient Solar Cells. *Science* **2017**, *356*, 1376–1379.

(2) Eperon, G. E.; Leijtens, T.; Bush, K. A.; Prasanna, R.; Green, T.; Wang, J. T.-W.; McMeekin, D. P.; Volonakis, G.; Milot, R. L.; May, R.; et al. Perovskite-Perovskite Tandem Photovoltaics with Optimized Band Gaps. *Science* **2016**, *354*, 861–865.

(3) Pisacane, V. L. *Fundamentals of Space Systems*; Oxford University Press, New York, 2005.

(4) Wehrenfennig, C.; Eperon, G. E.; Johnston, M. B.; Snaith, H. J.; Herz, L. M. High Charge Carrier Mobilities and Lifetimes in Organolead Trihalide Perovskites. *Adv. Mater.* **2014**, *26*, 1584–1589.

(5) Stranks, S. D.; Eperon, G. E.; Grancini, G.; Menelaou, C.; Alcocer, M. J. P.; Leijtens, T.; Herz, L. M.; Petrozza, A.; Snaith, H. J. Electron-Hole Diffusion Lengths Exceeding 1 Micrometer in an Organometal Trihalide Perovskite Absorber. *Science* **2013**, *342*, 341–344.

(6) Johnston, M. B.; Herz, L. M. Hybrid Perovskites for Photovoltaics: Charge-Carrier Recombination, Diffusion, and Radiative Efficiencies. *Acc. Chem. Res.* **2016**, *49*, 146–154.

(7) Ahn, N.; Son, D.-Y.; Jang, I.-H.; Kang, S. M.; Choi, M.; Park, N.-G. Highly Reproducible Perovskite Solar Cells with Average Efficiency of 18.3% and Best Efficiency of 19.7% Fabricated via Lewis Base Adduct of Lead(II) Iodide. *J. Am. Chem. Soc.* **2015**, *137*, 8696–8699.

(8) Noel, N. K.; Habisreutinger, S. N.; Wenger, B.; Klug, M. T.; Hörantner, M. T.; Johnston, M. B.; Nicholas, R. J.; Moore, D. T.; Snaith, H. J. A Low Viscosity, Low Boiling Point, Clean Solvent System for the Rapid Crystallisation of Highly Specular Perovskite Films. *Energy Environ. Sci.* **2017**, *10*, 145–152.

(9) Noel, N. K.; Congiu, M.; Ramadan, A. J.; Fearn, S.; McMeekin, D. P.; Patel, J. B.; Johnston, M. B.; Wenger, B.; Snaith, H. J. Unveiling the Influence of pH on the Crystallization of Hybrid Perovskites, Delivering Low Voltage Loss Photovoltaics. *Joule* **2017**, *1*, 328–343.

(10) Lin, Q.; Armin, A.; Nagiri, R. C. R.; Burn, P. L.; Meredith, P. Electro-Optics of Perovskite Solar Cells. *Nat. Photonics* **2014**, *9*, 106–112.

(11) Liu, M.; Johnston, M. B.; Snaith, H. J. Efficient Planar Heterojunction Perovskite Solar Cells by Vapour Deposition. *Nature* **2013**, *501*, 395–398.

(12) Hsiao, S.-Y.; Lin, H.-L.; Lee, W.-H.; Tsai, W.-L.; Chiang, K.-M.; Liao, W.-Y.; Ren-Wu, C.-Z.; Chen, C.-Y.; Lin, H.-W. Efficient All-Vacuum Deposited Perovskite Solar Cells by Controlling Reagent Partial Pressure in High Vacuum. *Adv. Mater.* **2016**, *28*, 7013–7019.

(13) Momblona, C.; Gil-Escrig, L.; Bandiello, E.; Hutter, E. M.; Sessolo, M.; Lederer, K.; Blochwitz-Nimoth, J.; Bolink, H. J. Efficient Vacuum Deposited P-I-N and N-I-P Perovskite Solar Cells Employing Doped Charge Transport Layers. *Energy Environ. Sci.* **2016**, *9*, 3456–3463.

(14) Patel, J. B.; Milot, R. L.; Wright, A. D.; Herz, L. M.; Johnston, M. B. Formation Dynamics of $CH_3NH_3PbI_3$ Perovskite Following Two-Step Layer Deposition. *J. Phys. Chem. Lett.* **2016**, *7*, 96–102.

(15) Jiang, Q.; Chu, Z.; Wang, P.; Yang, X.; Liu, H.; Wang, Y.; Yin, Z.; Wu, J.; Zhang, X.; You, J. Planar-Structure Perovskite Solar Cells with Efficiency beyond 21%. *Adv. Mater.* **2017**, *29*, 1703852.

(16) Patel, J. B.; Wong-Leung, J.; Van Reenen, S.; Sakai, N.; Wang, J. T. W.; Parrott, E. S.; Liu, M.; Snaith, H. J.; Herz, L. M.; Johnston, M. B. Influence of Interface Morphology on Hysteresis in Vapor-Deposited Perovskite Solar Cells. *Adv. Electron. Mater.* **2017**, *3*, 1600470.

(17) Milot, R. L.; Eperon, G. E.; Snaith, H. J.; Johnston, M. B.; Herz, L. M. Temperature-Dependent Charge-Carrier Dynamics in $CH_3NH_3PbI_3$ Perovskite Thin Films. *Adv. Funct. Mater.* **2015**, *25*, 6218–6227.

(18) Wehrenfennig, C.; Liu, M.; Snaith, H. J.; Johnston, M. B.; Herz, L. M. Charge Carrier Recombination Channels in the Low-

DOI: 10.1021/acs.jpclett.7b02935
J. Phys. Chem. Lett. 2018, 9, 263–268

Temperature Phase of Organic-Inorganic Lead Halide Perovskite Thin Films. *APL Mater.* **2014**, *2*, 081513.
(19) Brivio, F.; Frost, J. M.; Skelton, J. M.; Jackson, A. J.; Weber, O. J.; Weller, M. T.; Goñi, A. R.; Leguy, A. M. A.; Barnes, P. R. F.; Walsh, A. Lattice Dynamics and Vibrational Spectra of the Orthorhombic, Tetragonal, and Cubic Phases of Methylammonium Lead Iodide. *Phys. Rev. B: Condens. Matter Mater. Phys.* **2015**, *92*, 92.
(20) Zhang, H.; Qiao, X.; Shen, Y.; Moehl, T.; Zakeeruddin, S. M.; Grätzel, M.; Wang, M. Photovoltaic Behaviour of Lead Methylammonium Triiodide Perovskite Solar Cells down to 80 K. *J. Mater. Chem. A* **2015**, *3*, 11762−11767.
(21) Leong, W. L.; Ooi, Z.-E.; Sabba, D.; Yi, C.; Zakeeruddin, S. M.; Graetzel, M.; Gordon, J. M.; Katz, E. A.; Mathews, N. Identifying Fundamental Limitations in Halide Perovskite Solar Cells. *Adv. Mater.* **2016**, *28*, 2439−2445.
(22) Jacobsson, T. J.; Tress, W.; Correa-Baena, J.-P.; Edvinsson, T.; Hagfeldt, A. Room Temperature as a Goldilocks Environment for $CH_3NH_3PbI_3$ Perovskite Solar Cells: The Importance of Temperature on Device Performance. *J. Phys. Chem. C* **2016**, *120*, 11382−11393.
(23) Phuong, L. Q.; Nakaike, Y.; Wakamiya, A.; Kanemitsu, Y. Free Excitons and Exciton−Phonon Coupling in $CH_3NH_3PbI_3$ Single Crystals Revealed by Photocurrent and Photoluminescence Measurements at Low Temperatures. *J. Phys. Chem. Lett.* **2016**, *7*, 4905−4910.
(24) Wang, M.; Yim, W.-L.; Liao, P.; Shen, Y. Temperature Dependent Characteristics of Perovskite Solar Cells. *ChemistrySelect* **2017**, *2*, 4469−4477.
(25) Löper, P.; Pysch, D.; Richter, A.; Hermle, M.; Janz, S.; Zacharias, M.; Glunz, S. W. Analysis of the Temperature Dependence of the Open-Circuit Voltage. *Energy Procedia* **2012**, *27*, 135−142.
(26) Snaith, H. J.; Schmidt-Mende, L.; Grätzel, M.; Chiesa, M. Light Intensity, Temperature, and Thickness Dependence of the Open-Circuit Voltage in Solid-State Dye-Sensitized Solar Cells. *Phys. Rev. B: Condens. Matter Mater. Phys.* **2006**, *74*, 045306.
(27) Varshni, Y. P. Temperature Dependence of the Energy Gap in Semiconductors. *Physica* **1967**, *34*, 149−154.
(28) Hörmann, U.; Kraus, J.; Gruber, M.; Schuhmair, C.; Linderl, T.; Grob, S.; Kapfinger, S.; Klein, K.; Stutzman, M.; Krenner, H. J.; Brütting, W.; et al. Quantification of Energy Losses in Organic Solar Cells from Temperature-Dependent Device Characteristics. *Phys. Rev. B: Condens. Matter Mater. Phys.* **2013**, *88*, 235307.
(29) Sze, S. M. *Physics of Semiconductor Devices*, 2nd ed..; Wiley-Interscience: New York, 1981.
(30) Garcia-Belmonte, G. Temperature Dependence of Open-Circuit Voltage in Organic Solar Cells from Generation−recombination Kinetic Balance. *Sol. Energy Mater. Sol. Cells* **2010**, *94*, 2166−2169.
(31) Urbach, F. The Long-Wavelength Edge of Photographic Sensitivity and of the Electronic Absorption of Solids. *Phys. Rev.* **1953**, *92*, 1324−1324.
(32) Cody, G. D.; The Optical Absorption Edge of a-Si:H. *Semiconductors and Semimetals*, 1st ed.; Pankove, J. I., Ed.; Academic Press: Cambridge, 1984, Vol. *21*, Chapter 2, pp 11−82.
(33) Sumi, H.; Sumi, A. The Urbach-Martienssen Rule Revisited. *J. Phys. Soc. Jpn.* **1987**, *56*, 2211−2220.
(34) Cody, G. D.; Tiedje, T.; Abeles, B.; Brooks, B.; Goldstein, Y. Disorder and the Optical-Absorption Edge of Hydrogenated Amorphous Silicon. *Phys. Rev. Lett.* **1981**, *47*, 1480−1483.
(35) Gobinathan, R.; Hariharan, K.; Ramasamy, P. Electronic Absorption Spectra of Lead Iodide. *Krist. Tech.* **1981**, *16*, 1435−1438.
(36) Wright, A. D.; Verdi, C.; Milot, R. L.; Eperon, G. E.; Pérez-Osorio, M. A.; Snaith, H. J.; Giustino, F.; Johnston, M. B.; Herz, L. M. Electron−phonon Coupling in Hybrid Lead Halide Perovskites. *Nat. Commun.* **2016**, *7*, 11755.
(37) Herz, L. M. Charge-Carrier Mobilities in Metal Halide Perovskites: Fundamental Mechanisms and Limits. *ACS Energy Lett.* **2017**, *2*, 1539−1548.
(38) Coropceanu, V.; Cornil, J.; da Silva Filho, D. A.; Olivier, Y.; Silbey, R.; Brédas, J.-L. Charge Transport in Organic Semiconductors. *Chem. Rev.* **2007**, *107*, 926−952.
(39) Pope, M.; Swenberg, C. E. *Electronic Processes in Organic Crystals and Polymers*; Oxford University Press, New York, 1999.
(40) Roldán-Carmona, C.; Gratia, P.; Zimmermann, I.; Grancini, G.; Gao, P.; Graetzel, M.; Nazeeruddin, M. K. High Efficiency Methylammonium Lead Triiodide Perovskite Solar Cells: The Relevance of Non-Stoichiometric Precursors. *Energy Environ. Sci.* **2015**, *8*, 3550−3556.
(41) Jacobsson, T. J.; Correa-Baena, J.-P.; Halvani Anaraki, E.; Philippe, B.; Stranks, S. D.; Bouduban, M. E. F.; Tress, W.; Schenk, K.; Teuscher, J.; Moser, J.-E.; et al. Unreacted PbI_2 as a Double-Edged Sword for Enhancing the Performance of Perovskite Solar Cells. *J. Am. Chem. Soc.* **2016**, *138*, 10331−10343.
(42) Chen, Q.; Zhou, H.; Song, T.-B.; Luo, S.; Hong, Z.; Duan, H.-S.; Dou, L.; Liu, Y.; Yang, Y. Controllable Self-Induced Passivation of Hybrid Lead Iodide Perovskites toward High Performance Solar Cells. *Nano Lett.* **2014**, *14*, 4158−4163.
(43) Ahuja, R.; Arwin, H.; Ferreira da Silva, A.; Persson, C.; Osorio-Guillén, J. M.; Souza de Almeida, J.; Moyses Araujo, C.; Veje, E.; Veissid, N.; An, C. Y.; et al. Electronic and Optical Properties of Lead Iodide. *J. Appl. Phys.* **2002**, *92*, 7219−7224.
(44) Du, T.; Burgess, C. H.; Kim, J.; Zhang, J.; Durrant, J. R.; McLachlan, M. A. Formation, Location and Beneficial Role of PbI_2 in Lead Halide Perovskite Solar Cells. *Sustain. Energy Fuels* **2017**, *1*, 119−126.
(45) Shih, M.-C.; Li, S.-S.; Hsieh, C.-H.; Wang, Y.-C.; Yang, H.-D.; Chiu, Y.-P.; Chang, C.-S.; Chen, C.-W. Spatially Resolved Imaging on Photocarrier Generations and Band Alignments at Perovskite/PbI_2 Heterointerfaces of Perovskite Solar Cells by Light-Modulated Scanning Tunneling Microscopy. *Nano Lett.* **2017**, *17*, 1154−1160.
(46) Holovský, J.; De Wolf, S.; Werner, J.; Remeš, Z.; Müller, M.; Neykova, N.; Ledinský, M.; Černá, L.; Hrzina, P.; Löper, P.; et al. Photocurrent Spectroscopy of Perovskite Layers and Solar Cells: A Sensitive Probe of Material Degradation. *J. Phys. Chem. Lett.* **2017**, *8*, 838−843.
(47) Miyata, A.; Mitioglu, A.; Plochocka, P.; Portugall, O.; Wang, J. T.-W.; Stranks, S. D.; Snaith, H. J.; Nicholas, R. J. Direct Measurement of the Exciton Binding Energy and Effective Masses for Charge Carriers in Organic−inorganic Tri-Halide Perovskites. *Nat. Phys.* **2015**, *11*, 582−587.
(48) D'Innocenzo, V.; Grancini, G.; Alcocer, M. J. P.; Kandada, A. R. S.; Stranks, S. D.; Lee, M. M.; Lanzani, G.; Snaith, H. J.; Petrozza, A. Excitons versus Free Charges in Organo-Lead Tri-Halide Perovskites. *Nat. Commun.* **2014**, *5*, 3586.
(49) Saha, M. N. On a Physical Theory of Stellar Spectra. *Proc. R. Soc. London, Ser. A* **1921**, *99*, 135−153.
(50) Lin, Q.; Armin, A.; Burn, P. L.; Meredith, P. Filterless Narrowband Visible Photodetectors. *Nat. Photonics* **2015**, *9*, 687−694.
(51) Johnston, M. B. Optoelectronics: Colour-Selective Photodiodes. *Nat. Photonics* **2015**, *9*, 634−636.
(52) Burkhard, G. F.; Hoke, E. T.; McGehee, M. D. Accounting for Interference, Scattering, and Electrode Absorption to Make Accurate Internal Quantum Efficiency Measurements in Organic and Other Thin Solar Cells. *Adv. Mater.* **2010**, *22*, 3293−3297.
(53) Crothers, T. W.; Milot, R. L.; Patel, J. B.; Parrott, E. S.; Schlipf, J.; Müller-Buschbaum, P.; Johnston, M. B.; Herz, L. M. Photon Reabsorption Masks Intrinsic Bimolecular Charge-Carrier Recombination in $CH_3NH_3PbI_3$ Perovskite. *Nano Lett.* **2017**, *17*, 5782−5789.
(54) Fang, Y.; Dong, Q.; Shao, Y.; Yuan, Y.; Huang, J. Highly Narrowband Perovskite Single-Crystal Photodetectors Enabled by Surface-Charge Recombination. *Nat. Photonics* **2015**, *9*, 679−686.

DOI: 10.1021/acs.jpclett.7b02935
J. Phys. Chem. Lett. 2018, 9, 263−268